Regional Power System Black Start with Run-of-river Hydropower Plant and Battery Energy Storage

Weihang Yan, *Member*, *IEEE*, Vahan Gevorgian, *Fellow*, *IEEE*, Przemyslaw Koralewicz, *Member*, *IEEE*, S M Shafiul Alam, *Senior Member*, *IEEE*, and Emanuel Mendiola

***Abstract*—Battery energy storage systems (BESSs) are an important asset for power systems with high integration levels of renewable energy, and they can be controlled to provide various critical services to the power grid. This paper presents the real-world experience of using a megawatt-scale BESS with grid-following (GFL) and grid-forming (GFM) controls and a run-of-river (ROR) hydropower plant to restore a regional power system. To demonstrate this, we carry out power-hardware-in-the-loop experiments integrating an actual GFL- or GFM-controlled BESS and a load bank. Both the simulation and experimental results presented in this paper show the different roles of GFL- or GFM-controlled BESS in power system black starts. The results provide further insight for system operators on how GFL- or GFM-controlled BESS can enhance grid stability and how an ROR hydropower plant can be converted into a black-start-capable unit with the support of a small-capacity BESS. The results show that an ROR hydropower plant combined with a BESS has the potential of becoming one of enabling elements to perform bottom-up black-start schemes as opposed to conventional bottom-down method, thus enhancing the system resiliency and robustness.**

***Index Terms*—Run-of-river hydropower, battery energy storage system, grid-forming control, grid-following control, black start.**

I. Introduction

BATTERY energy storage systems (BESSs) have been recognized as one of the most critical units to ensure the reliable and flexible operation of power systems with high integration levels of renewable energy [1]. They provide a variety of ancillary services, ranging from long-duration power smoothing and reducing the curtailment of renewable energy, to short-term system frequency and voltage support [2] - [7]. Currently, the majority of the commissioned BESSs are operated in grid-following (GFL) mode, acting as current sources [8]. Although the BESSs themselves are not variable resources, they are interfaced with the grid through power electronics converters. The control flexibility of BESSs allows them to regulate the active and reactive power to the power grid and to provide various functions to enhance power system reliability, such as droop control and virtual inertia. These BESSs in GFL control mode have been demonstrated in large-scale BESS plants as well as wind and solar power plants [3], [5], [7]. Despite their easy control implementation, GFL inverters rely on the existence of a strong grid that is already formed by synchronous generators (SGs) to maintain system stability. They are incapable of providing any ancillary services during a power system blackout; hence, a BESS in GFL control mode cannot be used as a black-start resource even though the energy is readily available [8], [9].

Grid-forming (GFM) inverters have become a potential solution to maintain system stability in power grids with high levels of inverter-based resources (IBRs) where IBRs are controlled as voltage sources, similar to SGs. They are different from conventional GFL inverters, which "feed" the power grid formed by SGs [9], [10]. The North American Electric Reliability Corporation (NERC) states [11]: "GFM controls maintain an internal voltage phasor that is constant or nearly constant in the transient time frame. This allows the IBR to immediately respond to changes in the external system and maintain IBR control stability during challenging network conditions. The voltage phasor must be controlled to maintain synchronism with other devices in the power grid and must also regulate active and reactive power appropriately to support the power grid." The control and operation of IBRs in GFM control mode have attracted substantial attention from power system engineers, and significant efforts are now directed toward operating BESS, solar inverters, and onshore/offshore wind power plants in GFM control mode [12] - [21]. Various control methods have been proposed for GFM inverters, such as droop control, virtual synchronous machine, and virtual oscillator control [22] - [26].

Manuscript received: September 30, 2023; revised: February 13, 2024; accepted: April 16, 2024. Date of CrossCheck: April 16, 2024. Date of online publication: July 15, 2024.

This work was authored in part by the National Renewable Energy Laboratory, operated by Alliance for Sustainable Energy, LLC, for the U.S. Department of Energy (DOE) under Contract No. DE-AC36-08GO28308, and Battelle Energy Alliance, LLC under Contract No. DE-AC07-05ID14517 with the U.S. Department of Energy.

W. Yan (corresponding author), V. Gevorgian, P. Koralewicz, and E. Mendiola are with the National Renewable Energy Laboratory (NREL), Golden, CO 80401, USA (e-mail: weiahng.yan@nrel.gov; Vahan.Gevorgian@nrel.gov; przemyslaw.koralewicz@nrel.gov; emanuel.mendiola@nrel.gov).

S M S. Alam is with the Idaho National Laboratory (INL), Idaho Falls, USA (e-mail: smshafiul.alam@inl.gov).

DOI: 10.35833/MPCE.2023.000730

Droop control for GFM inverters is the simplest method to provide GFM functionality, and it has been proven as reliable and efficient for islanded operation [27]. It is expected that droop control for GFM inverters will be largely adopted by the industry for bulk power system applications [9], [28].

Despite the extensive interest in operating utility-scale BESS in GFM control mode, few research works have presented the practical experience and field demonstrations of GFM BESS [12], [29], [30]. This paper discusses and demonstrates the practical experience of using BESS in GFL and GFM control modes to improve power system restoration with a real-world example of a run-of-river (ROR) hydropower plant. ROR hydropower plants satisfy almost all major criteria to operate as black-start units − they are capable of operating in isochronous mode, and they are readily available because they require minimal time, fuel, and equipment to restart. But they suffer from inherent frequency stability issues when electric loads are being restored without the existence of a power grid [31]. Such issues in ROR hydropower plants have been observed in a black-start demonstration conducted by Idaho National Laboratory and Idaho Falls Power [32]. The demonstration identified that the excessive lowering of frequency nadirs in the ROR hydropower plant resulted in multiple generator trips during the network black-start process, wherein the hydropower governor played a major role in the system frequency instability. Therefore, the limited load-carrying capability of the hydropower generator complicates and prevents smooth power system restoration.

Research and industry applications have well demonstrated that BESS in GFL and GFM control modes and droop functions can stabilize the power system frequency by providing power compensation based on the measured frequency deviation [24]. Some research works have also noted that GFM inverters can more effectively mitigate power system frequency oscillations and improve the grid frequency nadir and rate-of-change-of-frequency than GFL inverters due to the direct power to frequency control [24], [33]; however, there are still many unanswered questions, including how BESS in GFL or GFM control mode can better support power system restoration services in coordination with other black-start units and how BESS should be placed in the network to better support a power system black start depending on their individual control modes.

This paper uses BESS to support the power system black start of a rural network using a 5.5 MVA ROR hydropower plant considering that the available capacity of the BESS is significantly smaller. For the system using a BESS in GFL control mode with droop control, the BESS cannot operate alone without first energizing part of the network; however, it is capable of providing critical damping to maintain the frequency stability of the ROR hydropower generator and to keep the SG online during the load restoration. Besides, for the system using a BESS in GFM control mode, the BESS can operate alone as a black-start unit and energize a portion of the critical load. It can be synchronized to the rest of the network which is simultaneously energized by the ROR hydropower generator. Therefore, the time of power system restoration is reduced by energizing the whole network in a parallel manner. We are also currently performing power-hardware-in-the-loop (PHIL) demonstrations on rural grid restoration using the ROR hydropower plant supported by an actual utility-scale BESS that can operate in either GFL or GFM control mode at the Flatirons Campus of the National Renewable Energy Laboratory (NREL) in Colorado, USA [34]. The detailed system test configurations are given in this paper. Both electromagnetic transient (EMT) simulations and PHIL tests reveal the different roles and damping characteristics of a BESS when it is operated in GFL or GFM control mode. The high-fidelity system demonstration provides further insight for utility operators on how an ROR hydropower plant can become a black-start-capable unit with the support of a small-capacity BESS. It also demonstrates the feasibility of the bottom-up black-start scheme with an ROR hydropower plant.

The rest of the paper is organized as follows. Section II presents the modeling and control of an ROR hydropower plant. It further pinpoints the root cause of its inherent frequency instability when the hydropower generator is performing load restoration. Section II also describes the GFL and GFM controls of a BESS. Section III introduces the PHIL test platform built around the 7 MW controllable grid interface (CGI), 3 MVA load bank, and 1 MW GFL/GFM BESS at NREL's Flatirons Campus. Section IV analyzes the results of the EMT simulations and PHIL demonstrations and further compares the power system black-start performance when a BESS is in different control modes. Section V concludes this paper.

II. Modeling of Hydropower Plant and BESS

A. RoR Hydropower Plant

The ROR hydropower generator studied in this paper uses a horizontal bulb-style Kaplan turbine, which is widely applied in low-head scenarios with moderate-to-high water flows. The H6E hydro governor model is used to represent a Kaplan turbine with a gate controller [35], [36], which can be selected to operate in either speed control mode or load control mode. To control an ROR hydropower generator as a black-start unit, the speed control mode is used, as shown in Fig. 1.

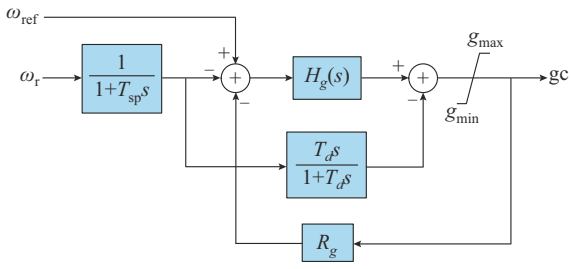

Fig. 1. Speed control mode of American Governor Company controller (H6E hydro governor).

The governor droop R_g is set as 0 p.u. if the ROR hydropower generator is the only black-start unit in the system. Here, the ROR hydropower generator is controlled in isochronous mode, where $\omega_{ref} = 1.0$ p.u.. ω_r denotes the rotor

speed of the SG. The proportional integral (PI) controller $H_g(s)$ is used to generate the gate position command gc and the derivative gain with low-pass filter. $T_d s/(1+T_d s)$ is a feed-forward signal to gc from the speed transducer. The gate servomotor responds to gc, which further adjusts the water flow, q, and the mechanical power, P_m, to the SG. Our previous black-start demonstration using the 8.9 MVA ROR hydropower plant [32] indicates a significant frequency nadir (up to 4 Hz) can be observed with a 0.5 MW load step. This is directly related to the low inertia and the hydro governor's slow response of the ROR hydropower generator. The demonstration also indicates that the tunning of governor control parameters can only lead to marginal improvement in generator's frequency response where under frequency relay may still trip during a load restoration. Due to the mechanical limitations of the hydropower governor device, the maximum gate actuator velocity, v_{elm}, is limited, which cannot support relatively large load steps that can be applied to the hydropower turbine while maintaining the stability of turbine speed. This further prohibits an ROR hydropower generator to become a black-start-capable unit without the frequency damping control from BESS. In Fig. 1, $g_{\max}$ and $g_{\min}$ are the maximum and minimum gate actuator strokes, respectively; and T_{sp} is the speed transducer time constant.

The lower path of Fig. 2 describes the turbine blade characteristics. The nonlinear characteristics of the gate position to the blades are modeled by a one-dimensional interpolation function as a lookup table with the output signal as bc. Similarly, the piecewise linearized characteristics of the water flow to power is modeled as a look-up table with the output signal as pgv. The parameters of the H6E hydro governor used in this paper are based on the field measurements of a plant, which are given in Appendix A Table AI in per-unit values. Detailed characteristics of the gate position to blade and the water flow to power are also given in Appendix A Fig. A1.

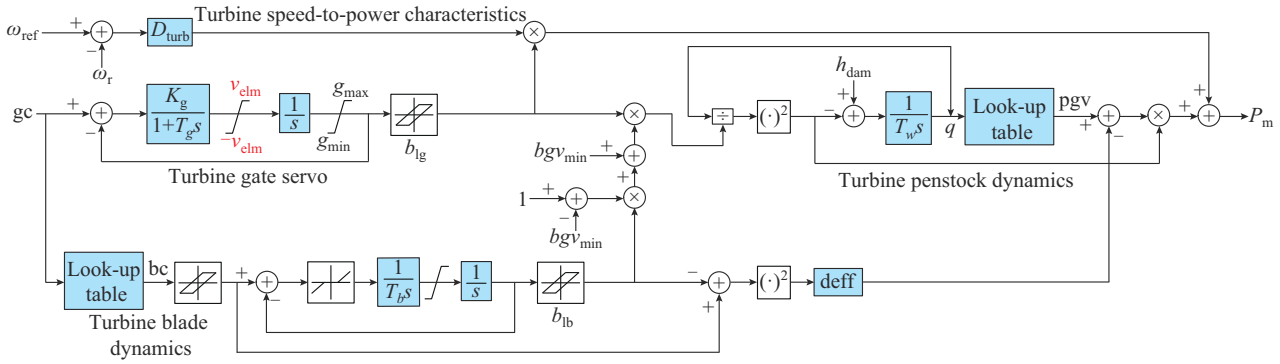

Fig. 2. System diagram of Kaplan turbine model.

B. GFM- or GFL-controlled BESS

Figure 3 shows the control diagrams of a single-stage BESS in GFL and GFM control modes, as described in [9] and [10]. v_{dq} and i_{dq} are the voltage and current feedbacks of the BESS outputs, respectively, after the abc-dq transform. Modulation signals, m_{abc}, are used to generate the pulse width modulation (PWM) signals and drive the three-phase voltage source converter. Figure 3(a) and (b) shows the outer-loop controls of the BESS in GFL and GFM control modes, respectively. Here, P_{ref} and Q_{ref} are the power references, and the instantaneous active and reactive power outputs are denoted as P and Q, accordingly. The inner-loop current control, illustrated in Fig. 3(c), is identical for both GFL and GFM controls.

In GFL control mode of the BESS, the outer-loop PI compensators, $H_p(s)$, control the active and reactive power at the point of common coupling (PCC) of the BESS, and they further generate the current references, $i_{d,\text{ref}}$ and $i_{q,\text{ref}}$, for the inner-loop current controllers, $H_i(s)$. A phase-locked loop (PLL) is used to obtain the grid voltage angle, θ_{PLL}, required for converter synchronization. Besides, in GFM control mode, the voltage control, $H_v(s)$, is implemented on top of the current control instead of the power control as in GFL control mode. The current references, $i_{d,\text{ref}}$ and $i_{q,\text{ref}}$, are generated to regulate the converter output currents, and they can provide a current-limiting function. The decoupling terms are $K_{\text{di}} = 2\pi f_1 L$ and $K_{\text{dv}} = 2\pi f_1 C$, where the fundamental frequency, f_1, equals 60 Hz, and the inductance and capacitance of the LC filter are denoted as L and C, respectively. The reference for the q-axis component of the voltage, $v_{q,\text{ref}}$, is set to be 0 in GFM control mode for simplicity; hence, the voltage reference on the d-axis, $v_{d,\text{ref}}$, represents the reference magnitude of the PCC voltages of the BESS. The frequency of the BESS is controlled by the droop characteristics, and it further adds a nominal angular frequency to derive phase θ. The active power-frequency and reactive power-voltage droop controls are implemented as active and reactive power loops, with droop coefficients of D_p and D_q, respectively.

Alternatively, the inner-loop current control can be eliminated for the BESS in GFM control mode [24], [37], where the voltage controller, $H_v(s)$, directly regulates m_{abc} and further controls the PCC voltages of the BESS. In such GFM control implementation, virtual impedances are required to adjust the voltage references of the BESS based on the current feedback for fault current-limiting control. The droop control remains the same.

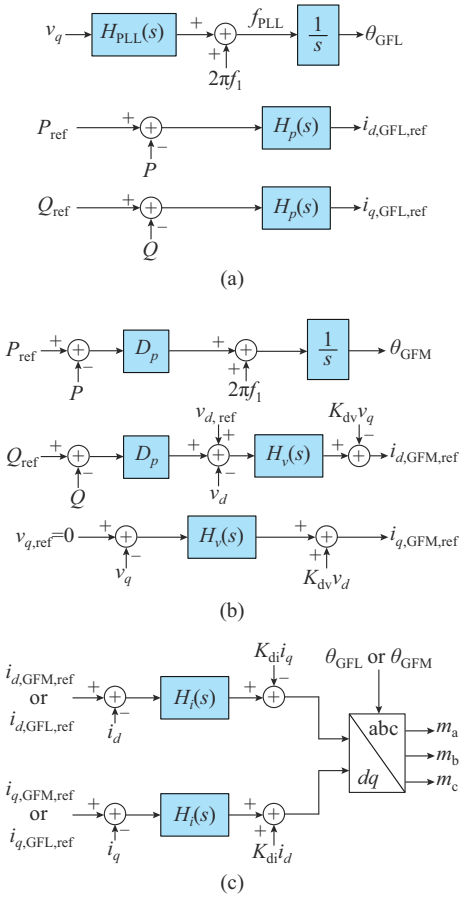

Fig. 3. BESS inverter control diagrams. (a) Outer-loop control of BESS in GFL control mode. (b) Outer-loop control of BESS in GFM control mode. (c) Inner-loop control of BESS for both GFL and GFM control modes.

III. NREL PHIL Experimental Platform

This section presents NREL PHIL experimental platform used for the demonstration of power system black start. The main test apparatus at the Flatirons Campus, as shown in Fig. 4, is set up around the 7 MVA CGI [29], [30], [34]. The CGI is a back-to-back converter that operates at nominal 13.2 kV medium voltage on its test terminals, which represent a full four-wire point of interconnection for any inverter under test. The fast response time of the CGI (less than 1 ms), CGI ability to control voltages individually in each phase, and high overcurrent capability of CGI (7 times the rated current) give a unique platform for the test and validation of inverter-based systems under fully controlled grid conditions. The CGI is capable of emulating balanced and unbalanced low- and high-voltage conditions of various durations on its medium-voltage terminals, frequency deviations, and phase jumps, and it is capable of injecting the desired harmonic content. The CGI is connected to a 13.2 kV underground collector system at NREL's test site, allowing for quick interconnection with multi-megawatt generation resources, energy storage, and loads located at the site. Here, the CGI provides an isolation between the test grid and the utility grid, such that any faults or transient events applied on the equipment under test do not impact other generations and loads at the test site [30].

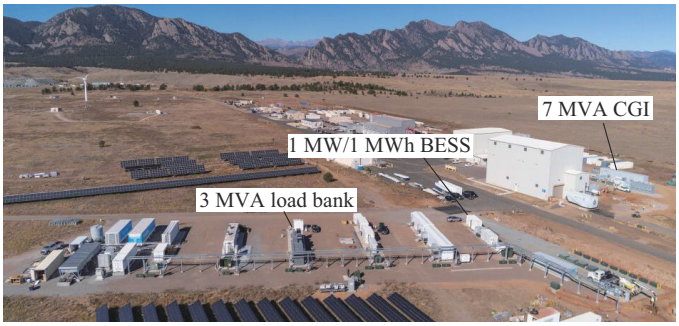

Fig. 4. Aerial view of test apparatus at NREL's Flatirons Campus.

The components used in the PHIL demonstrations described in this paper include: ① a 1 MW/1 MWh BESS with a 2.2 MVA inverter with frequency and voltage droop control that can operate in either GFL or GFM control mode; ② a 3 MVA R-L-C load bank; and ③ a real-time digital simulator (RTDS) rack for simulating the power system network and controlling the CGI as the PHIL interface. All these devices are interconnected with the 13.2 kV system via step-up transformers. An additional grounding transformer was connected to provide a ground reference in islanded mode. The overall single line diagram of the setup is shown in Fig. 5, where CB is short for circuit breaker. It is worth noting that this paper uses thicker lines to represent buses with higher voltage levels. The red line with arrows in Fig. 5 denotes control signals between CGI and RTDS. The system is equipped with a high-speed (50 kHz) distributed synchronized data acquisition system deployed in every node of the medium voltage network. Voltage and current waveforms were captured in each node and then used to calculate the power time series.

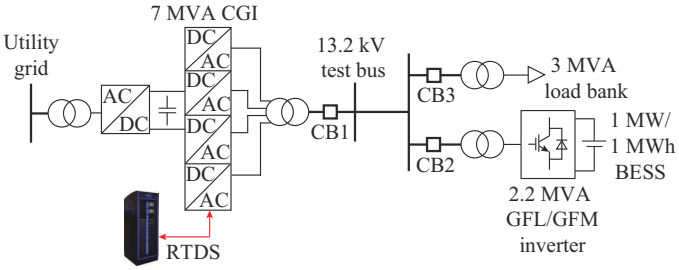

Fig. 5. High-fidelity PHIL test setup of multi-megawatt system at NREL.

Note that the droop settings of the BESS inverter in both GFM and GFL control modes are calculated in per unit based on the rating of 1 MW of the BESS instead of the rating of the inverter. This is done to stay consistent with the actual active power rating of the whole BESS system. The detailed control parameters of the BESS are given in Appendix A Table AII.

IV. System Simulation and PHIL Validation

To demonstrate how a BESS in GFL or GFM control mode can support the power system black start with an ROR hydropower generator, EMT simulations in RSCAD and PHIL demonstrations are carried out in this section. We consider a rural power system network in the eastern part of Ida-

ho, USA, where the ROR hydropower plant is commissioned [38]. Specifically, a 5.5 MVA ROR hydropower generator with an H6E hydro governor (modeled in Fig. 1 and Fig. 2) is connected at the Badger substation through underground cables and step-up transformers, which acts as one of the black-start units in the power system. Here, we consider that the ROR hydropower generator is controlled to soft start the Badger substation, the Tetonia substation, the Targhee substation, and the load bus. As a result, the terminal voltage of the SG is controlled to ramp up from 0 p.u. to the nominal value to prevent inrush currents of transformers. The identified critical load is 1.187 MW, and it is located at the load bus in the Targhee substation.

This paper considers three cases. Case 1 (base case) evaluates the black-start performance of the ROR hydropower generator without the support of a BESS. Case 2 evaluates the black-start performance of the ROR hydropower generator with the support of a BESS in GFL control mode. Case 3 evaluates the black-start performance of the ROR hydropower generator with the support of a BESS in GFM control mode. A 500 kW BESS (inverter capacity is scaled down by the CGI) in GFL and GFM control modes is considered for Cases 2 and 3, respectively. Given that the capacity of the BESS is significantly smaller than the SG, it mainly supports the ROR hydropower generator in the power system black start and provides frequency damping control. To enable the droop function in the BESS in GFL control mode, the active power reference, P_{ref}, is regulated as in (1) based on the measured frequency deviation between the nominal frequency, f_1, and the BESS measured frequency using a PLL, f_{PLL}, at the PCC of BESS.

$$P_{\text{ref}} = \mathrm{e}^{-\tau s}\frac{1}{D_p}[f_1 - G_p(s)f_{\text{PLL}}] + P_{\text{ref},0} \tag{1}$$

where τ is the communication delay; and $P_{\text{ref},0}$ is the initial power dispatch of the BESS. Besides, a droop-controlled BESS in GFM control mode naturally controls the power of inverter based on the frequency deviation, as presented in Fig. 3(b). Here, $D_p = 0.05$ p.u..

A. EMT Simulation in RSCAD

First, EMT simulations are carried out in RSCAD for all three cases. Specifically, the EMT simulations evaluate how the BESS in different control modes at various locations can impact the performance of the power system black start. It is well studied that a BESS in GFL control mode behaves as a current source in the network. It cannot operate without a power grid formed by SGs. As a result, in Case 2, the BESS in GFL control mode can only support the power system black start and can start providing frequency damping control once the BESS-connected bus is energized. In other words, placing the BESS in GFL control mode adjacent to the hydropower plant can provide stability enhancement functions in the early stage of the system restoration process.

In Case 3, a BESS in GFM control mode is controlled to behave as a voltage source in the network. It can form the power grid without the need for an energized bus. The droop-controlled BESS in GFM control mode can naturally respond to system frequency and voltage variations; hence, it can better support in the power system black start when it is placed near the critical load. In such cases, BESS in GFM control mode can energize a portion of the critical load (due to the capacity limitation) and decrease the load step on the hydropower generator. Meanwhile, the hydropower generator can energize the rest of the network connected to the Targhee substation, which significantly reduces the required time of power system black start. Besides, a BESS in GFM control mode can also provide critical damping control to an utility grid when it is adjacent to the load center during normal operation. However, it should be noted that the synchronization check function should be enabled for breaker 5 (BRK5) in Fig. 6 to smoothly synchronize two networks formed by the SG and the BESS.

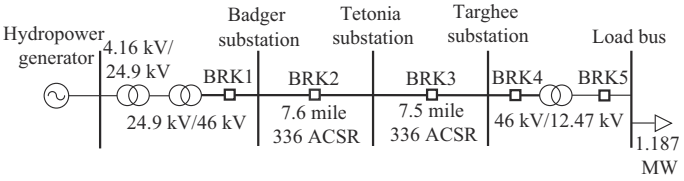

Fig. 6. Topology of regional power system network for black-start study.

Figure 7(a) compares the frequency responses of the hydropower generator for Cases 1, 2, and 3. Here, we consider the example of connecting the BESS near the hydropower plant.

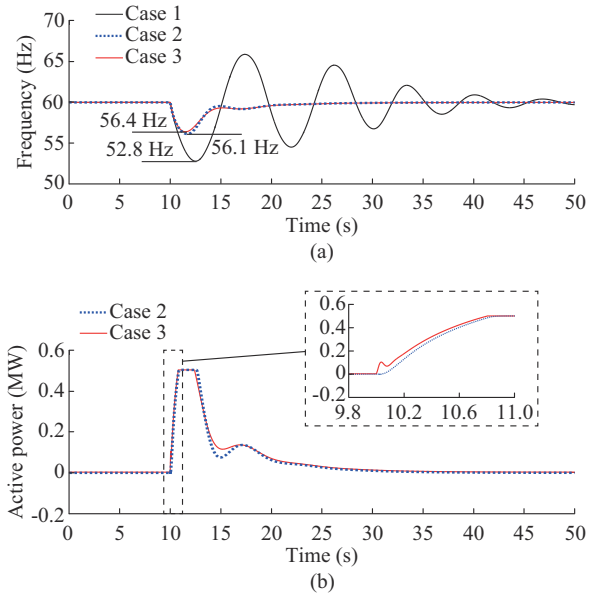

Fig. 7. Case comparison. (a). Frequency response of hydropower generator. (b). Active power response of BESS during power system black start.

With the mechanical limitation on the maximum gate actuator velocity and the machine inertia, in Case 1, the hydropower generator undergoes a severe frequency oscillation with a frequency nadir of 52.81 Hz when restoring the critical load (closing BRK5). The settling time of the frequency oscillation of the turbine is 37.5 s. Cases 2 and 3 clearly show the frequency damping characteristics from the BESS with different control modes, where the frequency nadirs reduce to 56.14 Hz and 56.42 Hz in GFL and GFM control modes, respectively. The frequency settling time for both cases is reduced to 13.2 s. Meanwhile, in Case 3, the BESS in

GFM control mode can provide better frequency damping control than the BESS in GFL control mode using the same droop coefficient. This is because GFM control directly regulates the frequency of the inverter based on power feedback.

Table I summarizes the performance of the power system black start when the BESS is placed at different locations of the network. As a result, the location of the BESS in GFL control mode does not impact the turbine frequency oscillation much; however, it can start providing frequency damping control for the SG early in the power system black-start process if it is placed near the hydropower plant, reducing the risk of a generator underfrequency trip-off. The BESS in GFM control mode can more efficiently contribute to the power system black start when it is connected to the load bus. Two GFM units (SG and BESS) can simultaneously energize the network, reducing the load step applied on the hydropower turbine. The controlled synchronization between the SG-formed grid and the BESS-formed grid also introduces the minimum frequency transients (frequency nadir of 59.93 Hz and settling time of 0 s), de-risking the frequency stability of the ROR hydropower generator (the limits for closing BRK5 refer to [39], [40]). BESS with GFL control are known to experience high frequency resonance when they are connected to a weak power grid [9]. Such characteristics prevent a BESS in GFL control mode from being installed far from the hydropower plant when considering the requirements of power system black starts. BESS in GFM control mode does not have such concerns.

TABLE I
PERFORMANCE OF POWER SYSTEM BLACK START WITH DIFFERENT BESS CONFIGURATIONS

BESS location	Case 2		Case 3	
	Frequency nadir (Hz)	Settling time (s)	Frequency nadir (Hz)	Settling time (s)
Hydropower plant	56.14	13.2	56.42	13.0
Badger substation	56.12	13.3	56.39	13.1
Tetonia substation	56.12	13.3	56.39	13.1
Targhee substation	53.26	8.4	59.93/57.67	0/6.4

B. PHIL Demonstration

This subsection presents the results of the PHIL demonstrations studied in this paper, where the BESS uses the 1 MW, 1 MWh battery with the GFL or GFM inverters at NREL's Flatirons Campus. To represent a 500 kW BESS in the PHIL demonstration, a scaling factor of 0.5 is implemented in the CGI to scale down the capacity of the BESS in the real-time simulations. Figure 8 explains the PHIL setup for Cases 2 and 3. Specifically, Case 2 integrates the BESS in GFL control mode through the CGI at the 4.16 kV bus of the hydropower plant, and Case 3 integrates the GFM BESS and the 3 MVA load bank through the CGI at the 12.47 kV load bus; hence, Case 3 can represent a small-scale microgrid formed by the BESS in GFM control mode before it is synchronized to the main power grid. The network outside the dashed box in Fig. 8 remains the same for the EMT simulations and PHIL demonstrations. The network is simulated in RTDS.

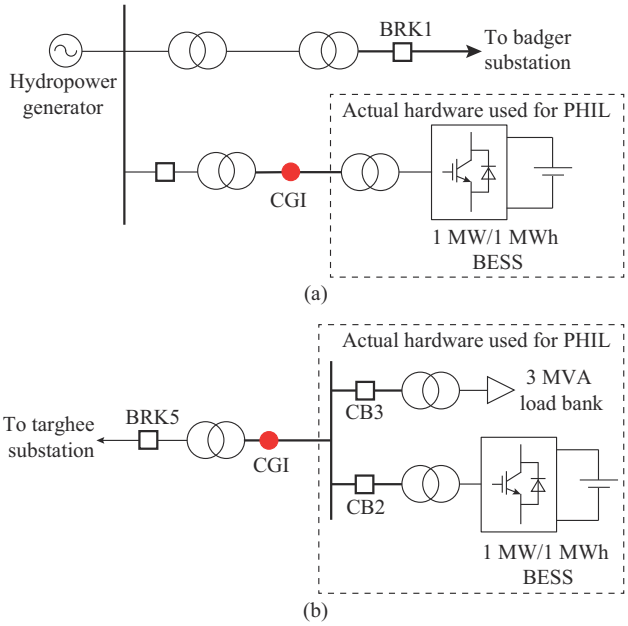

Fig. 8. PHIL system setup. (a) Case 2. (b) Case 3.

The PHIL demonstration presented in Fig. 9 and Fig. 10 shows the feasibility of using a BESS in GFL or GFM control mode to convert an ROR hydropower generator into a black-start-capable unit. Similar to the EMT simulations, the frequency nadir of the SG is significantly reduced with the support of the BESS. The BESS reduces the risk of a generator underfrequency trip-off; meanwhile, the frequency oscillations of the turbine can also be effectively damped with the stabilization from the BESS. Because the hydropower generator is operated in isochronous mode, the steady-state power of a droop-controlled BESS (both GFL and GFM) can return to 0; hence, the energy consumption for the frequency damping control of BESS is negligible, and there is no concern about the state of charge of the battery. Besides, the soft start of the network (voltage ramp up) reduces the inrush currents during the transformer energization, and the controlled BESS synchronization also brings the minimum disturbance to the SG, resulting in a smooth power system black start.

Note that the BESS in GFM control mode forms the power grid for a portion of the critical load (it operates as an islanded microgrid) before it is synchronized to the main power grid. The secondary frequency control of the BESS in GFM control mode is not considered in Case 3. As a result, the BESS operator needs to manually adjust the power reference of the BESS in GFM control mode to control the frequency of the load bank to 60 Hz. During this process, we can observe that the frequency of the BESS in GFM control mode starts with 58.6 Hz after being deblocked, and it returns to 60.1 Hz and then 60.02 Hz after manually adjusting the active power reference. The frequency of the SG is maintained as 60 Hz during this process. The voltage oscillation observed on the load bank is due to the measurement error caused by the frequency shift (58.6 Hz). Figure 10 further presents the active power responses of the experimental BESS in GFL or GFM control mode when the critical load is restored.

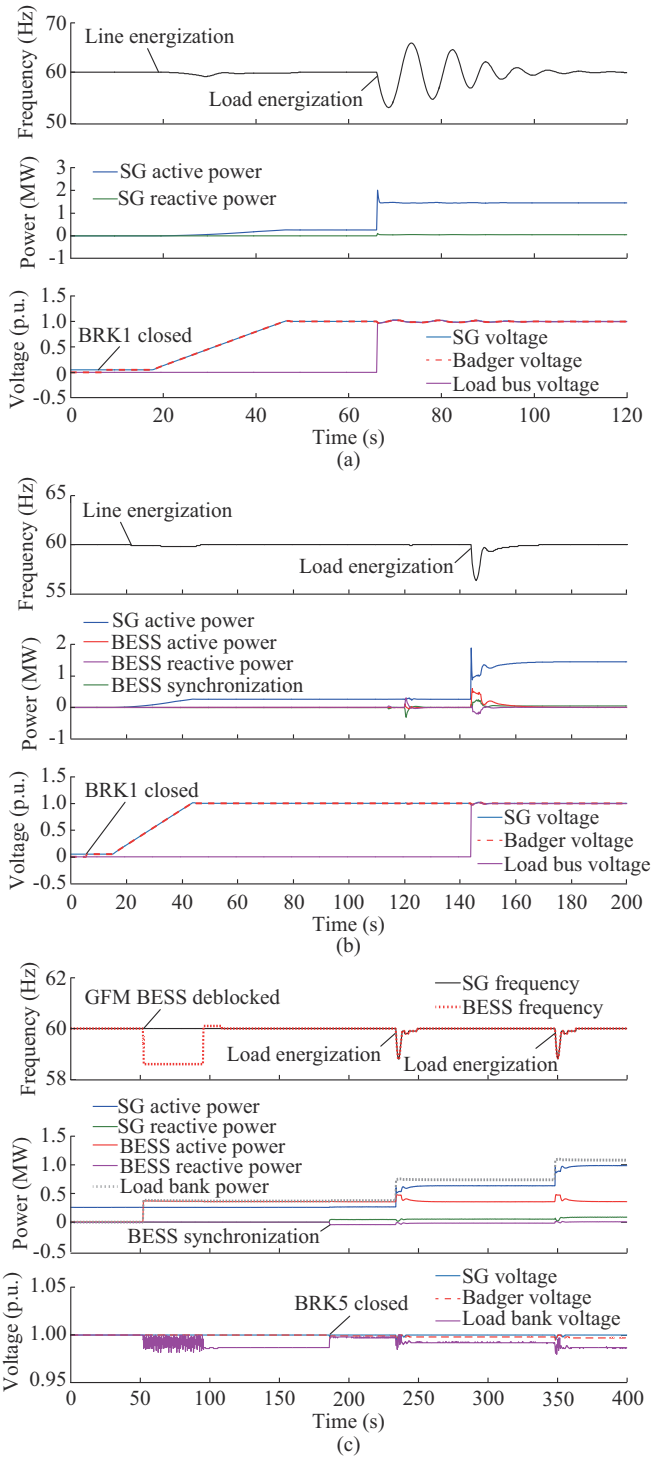

Fig. 9. PHIL demonstrations of regional power system black start using hydropower generator and BESS. (a) Case 1. (b) Case 2. (c) Case 3.

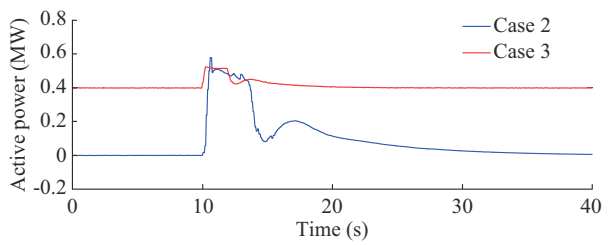

Fig. 10. PHIL active power response of megawatt-scale BESS.

C. Test Result Discussion

Both the EMT simulations and PHIL demonstrations presented in this paper show that a small-capacity BESS in GFL or GFM control mode can significantly reduce the risk of hydropower generator trips during the energization of the critical load.

The test results are qualitatively similar; however, some factors can still cause differences between the EMT simulations and PHIL demonstrations. First, the design of inverter control parameter is considered as vendor proprietary information; hence, comparing it to the developed BESS models in EMT simulation does not yield valuable information. Second, the power limiting control of the experimental BESS at NREL is not ideal (particularly for BESS in GFL control mode), where the power overshoot can reach 0.6 MW. Third, the BESS operator can only set the droop coefficients for the experimental BESS, whereas the parameters of the inverter internal control cannot be modified (causing differences compared with simulated BESS). Finally, it is difficult to determine the communication delay, τ, between the plant controller and the BESS inverter control in field tests, and it is assumed to be 20 ms for simplicity in the EMT simulations. Nevertheless, the PHIL tests performed in this paper demonstrate that the existing commercialized BESS in GFM or GFL control mode can provide critical damping to support power system restoration and can black start a portion of the network in GFM mode. The tests further verify the validity and practicability of the BESS model developed in EMT simulations.

V. Conclusion

In this paper, we present a real-world demonstration of how a megawatt-scale BESS in GFL or GFM control mode can be used to facilitate power system restoration. We show that a 5.5 MVA ROR hydropower plant can be converted into a black-start-capable unit with a small-capacity BESS despite its inherent frequency stability issues. For the system using a BESS in GFL mode with droop control, the BESS cannot operate alone without first energizing part of the network. However, it is capable of providing critical damping to maintain the frequency stability of the ROR hydropower generator. Besides, for the system using a BESS in GFM control mode, the BESS can operate alone as a black-start unit and can energize a portion of the critical load. Then, it can be synchronized to the rest of the network formed by the ROR hydropower generator, in a seamless manner, which reduces the required time of the power system restoration. The controlled network synchronization has a negligible impact on the hydropower generator.

We also perform PHIL demonstrations on a rural grid restoration using the ROR hydropower plant supported by an actual utility-scale BESS that can operate in either GFL or GFM control mode at NREL. Both EMT simulations and PHIL tests support the analysis in this paper. The PHIL test results also validate the practicability of the BESS in the EMT model. They provide further insight for system opera-

tors on how a commercial BESS in GFL or GFM control mode can enhance grid stability and how a ROR hydropower plant can be converted into a black-start-capable unit with the support of a small-capacity BESS. An ROR hydropower plant combined with a BESS can have the potential to improve system resiliency by performing bottom-up system black start, as opposed to conventional bottom-down method.

APPENDIX A

This section presents the system parameters required for the EMT simulations and PHIL demonstrations.

TABLE AI
PARAMETERS OF HYDROPOWER GOVERNOR

Parameter	Value
Turbine rated power	5.5 MW
Generator rated power	6 MW
Generator inertia constant	1 s
Penstock water time constant T_w	0.87 s
Operating head h_{dam}	1 p.u.
R_g	0 p.u.
T_{sp}	0.02 s
$H_g(s)$	$1.61+0.39/s$
Governor derivative gain K_{d}	0.675 p.u.
Derivative time constant T_d	0.05 s
Turbine gate servo time constant T_g	0.025 s
Turbine gate servo gain K_g	1 p.u.
$g_{\max}$	1 p.u.
$g_{\min}$	0 p.u.
v_{elm}	(0.05 p.u.)·s^{-1}
Blade servo time constant T_b	0.01 s
Flow area factor of blades at minimum position $bgv_{\min}$	0 p.u.
Backlash in ring linkage b_{lg}	0 p.u.
Off-blade angle power decrease factor deff	0 p.u.
Turbine speed sensitivity constant D_{turb}	0 p.u.

TABLE AII
PARAMETERS OF BESS WITH GFM AND GFL CONTROLS

Parameter	Value
BESS rated power	1 MW
Battery DC voltage	850 V
Converter rated AC voltage V_1	400 V
f_1	60 Hz
$G_p(s)$	$1/(0.02s+1)$
$H_i(s)$	$0.000255+1/(3.27s)$
L	0.3 mH
C	22 μF
$H_v(s)$	$D_p=0.05$ p.u.; $D_q=0.05$ p.u.
GFM voltage compensator	$12.16+1/(0.017s)$
GFL power compensator $H_p(s)$	$0.000735+1/(28.529s)$
PLL compensator $H_{\text{PLL}}(s)$	$0.237+1/(0.0224s)$

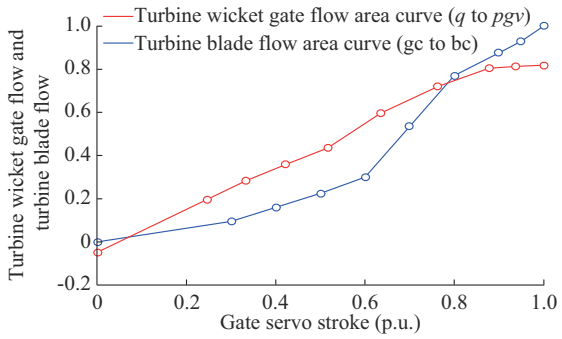

Fig. A1. Piecewise linearization of blade versus gate command and power versus water flow.

REFERENCES

[1] X. Li and S. Wang, "Energy management and operational control methods for grid battery energy storage systems," *CSEE Journal of Power and Energy Systems*, vol. 7, no. 5, pp. 1026-1040, Sept. 2021.
[2] X. Li, D. Hui, and X. Lai, "Battery energy storage station (BESS)-based smoothing control of photovoltaic (PV) and wind power generation fluctuations," *IEEE Transactions on Sustainable Energy*, vol. 4, no. 2, pp. 464-473, Apr. 2013.
[3] J. Tan and Y. Zhang, "Coordinated control strategy of a battery energy storage system to support a wind power plant providing multi-timescale frequency ancillary services," *IEEE Transactions on Sustainable Energy*, vol. 8, no. 3, pp. 1140-1153, Jul. 2017.
[4] X. Wang, T. Zhao, and A. Parisio, "Frequency regulation and congestion management by virtual storage plants," *Sustainable Energy Grids & Networks*, vol. 29, p. 100586, Mar. 2022.
[5] Z. Wu, D. W. Gao, H. Zhang *et al.*, "Coordinated control strategy of battery energy storage system and PMSG-WTG to enhance system frequency regulation capability," *IEEE Transactions on Sustainable Energy*, vol. 8, no. 3, pp. 1130-1143, Jul. 2017.
[6] Y.-S. Kim, E.-S. Kim, and S.-I. Moon, "Frequency and voltage control strategy of standalone microgrids with high penetration of intermittent renewable generation systems," *IEEE Transactions on Power Systems*, vol. 31, no. 1, pp. 718-728, Jan. 2016.
[7] W. Yan, X. Wang, W. Gao *et al.*, "Electro-mechanical modeling of wind turbine and energy storage systems with enhanced inertial response," *Journal of Modern Power Systems and Clean Energy*, vol. 8, no. 5, pp. 820-830, Sept. 2020.
[8] B. Kroposki, A. Bernstein, J. King *et al.*, "Autonomous energy grids: controlling the future grid with large amounts of distributed energy resources," *IEEE Power and Energy Magazine*, vol. 18, no. 6, pp. 37-46, Nov.-Dec. 2020.
[9] W. Yan, S. Shah, V. Gevorgian *et al.*, "Sequence impedance modeling of grid-forming inverters," in *Proceedings of IEEE PES General Meeting*, Washington DC, USA, Jul. 2021, pp. 1-5.
[10] ESIG High Share of Inverter-Based Generation TaskForce. (2022, Mar.). Grid-forming technology in energy systems integration. [Online]. Available: https://www. esig. energy/wp-content/uploads/2022/03/ESIG-GFM-report-2022.pdf
[11] North American Electric Reliability Corporation. (2021, Jan.). Grid forming technology: bulk power system reliability considerations. [Online]. Available: https://www.nerc.com/comm/RSTC_Reliability_Guidelines/White_Paper_Grid_Forming_Technology.pdf.
[12] S. Rao, S. Dutta, M. Lwin *et al.*, "Grid forming inverters real life implementation experience and lessons learned," in *Proceedings of 9th Renewable Power Generation Conference*, Dublin, Ireland, Mar. 2021, pp. 7-12.
[13] S. Cherevatskiy, S. Sproul, S. Zabihi *et al.*, "Grid forming energy storage system addresses challenges of grids with high penetration of renewables (a case study)," in *Proceedings of Wind Integration Workshop*, Dublin, Ireland, Oct. 2019, pp. 1-10.
[14] X. Quan, R. Yu, X. Zhao *et al.*, "Photovoltaic synchronous generator: architecture and control strategy for a grid-forming PV energy system," *IEEE Journal of Emerging and Selected Topics in Power Electronics*, vol. 8, no. 2, pp. 936-948, Jun. 2020.
[15] B. Pawar, E. I. Batzelis, S. Chakrabarti *et al.*, "Grid-forming control for solar PV systems with power reserves," *IEEE Transactions on Sustainable Energy*, vol. 12, no. 4, pp. 1947-1959, Oct. 2021.
[16] A. Roscoe, P. Brogan, D. Elliott *et al.*, "Practical experience of operat-

ing a grid forming wind park and its response to system events," in *Proceedings of Wind Integration Workshop*, Dublin, Ireland, Oct. 2019, pp. 1-8.
[17] A. Roscoe, P. Brogan, D. Elliott *et al*., "Practical experience of providing enhanced grid forming services from an onshore wind park," in *Proceedings of Wind Integration Workshop*, Virtual conference, Nov. 2020, pp. 1-10.
[18] V. Gevorgian, S. Shah, W. Yan *et al*., "Grid-forming wind: getting ready for prime time, with or without inverters," *IEEE Electrification Magazine*, vol. 10, no. 1, pp. 52-64, Mar. 2022.
[19] W. Yan, S. Shah, V. Gevorgian *et al*., "On the low risk of SSR in type III wind turbines operating with grid-forming control," *IEEE Transactions on Sustainable Energy*, vol. 15, no. 1, pp. 443-453, Jan. 2024.
[20] P. Huang and L. Vanfretti, "Adaptive damping control of MMC to suppress high-frequency resonance," *IEEE Transactions on Industrial Application*, vol. 59, no. 6, pp. 7224-7237, Nov.-Dec. 2023.
[21] P. Huang and L. Vanfretti, "Multi-tuned narrowband damping for suppressing MMC high-frequency oscillations," *IEEE Transactions on Power Delivery*, vol. 38, no. 6, pp. 3804-3819, Dec. 2023.
[22] J. Rocabert, A. Luna, F. Blaabjerg *et al*., "Control of power converters in AC microgrids," *IEEE Transactions on Power Electronics*, vol. 27, no. 11, pp. 4734-4749, Nov. 2012.
[23] J. Liu, Y. Miura, and T. Ise, "Comparison of dynamic characteristics between virtual synchronous generator and droop control in inverter-based distributed generators," *IEEE Transactions on Power Electronics*, vol. 31, no. 5, pp. 3600-3611, May 2016.
[24] W. Yan, L. Cheng, S. Yan *et al*., "Enabling and evaluation of inertial control for PMSG-WTG using synchronverter with multiple virtual rotating masses in microgrid," *IEEE Transactions on Sustainable Energy*, vol. 11, no. 2, pp. 1078-1088, Apr. 2020.
[25] Y. Xu, H. Nian, B. Hu *et al*., "Impedance modeling and stability analysis of VSG controlled Type-IV wind turbine system," *IEEE Transactions on Energy Conversion*, vol. 36, no. 4, pp. 3438-3448, Dec. 2021.
[26] B. B. Johnson, S. V. Dhople, J. L. Cale *et al*., "Oscillator-based inverter control for islanded three-phase microgrids," *IEEE Journal of Photovoltaics*, vol. 4, no. 1, pp. 387-395, Jan. 2014.
[27] R. Panora, J. E. Gehret, M. M. Furse *et al*., "Real-world performance of a CERTS microgrid in Manhattan," *IEEE Transactions on Sustainable Energy*, vol. 5, no. 4, pp. 1356-1360, Oct. 2014.
[28] North American Electric Reliability Corporation. (2023, Jan.). Grid forming functional specifications for BPS-connected battery energy storage systems. [Online]. Available: https://www. nerc. com/comm/RSTC_Reliability_Guidelines/White_Paper_GFM_Functional_Specifi - cation.pdf.
[29] V. Gevorgian, P. Koralewicz, S.l Sha *et al*., "Photovoltaic plant and battery energy storage system integration at NREL's Flatirons Campus," National Renewable Energy Laboratory, Golden, CO, Tech. Rep. NREL/TP-5D00-81104, 2022.
[30] V. Gevorgian, P. Koralewicz, S. Shah *et al*., "Testing GFM and GFL inverters operating with synchronous condenser," in *Proceedings of IEEE PES General Meeting*, Orlando, USA, Jul. 2023, pp. 1-5.
[31] S. M. S. Alam, R. Bhattarai, T. Hussain *et al*., "Enhancing local grid resilience with small hydropower hybrids – proving the concept through demonstration, simulation, and analysis with Idaho Falls Power," Idaho National Laboratory, Idaho Falls, ID, Tech. Rep. INL/RPT-22-69038, 2022.
[32] S. M. S. Alam, A. Banerjee, C. Loughmiller *et al*., "Idaho falls power black start field demonstration – preliminary outcomes report," Idaho National Laboratory, Idaho Falls, ID, Tech. Rep. INL/EXT-21-63855, 2021.
[33] D. Pattabiraman, J. Tan, V. Gevorgian *et al*., "Impact of frequency-watt control on the dynamics of a high DER penetration power system," in *Proceedings of IEEE PES General Meeting*, Portland, USA, Aug. 2018, pp. 1-5.
[34] V. Gevorgian, P. Koralewicz, H. Pico *et al*., "Wgrid-49 GMLC project report: understanding the role of short-term energy storage and large motor loads for active power controls by wind power," National Renewable Energy Laboratory, Golden, CO, Tech. Rep. NREL/TP-5D00-72888, 2019.
[35] A. Banerjee, S. M. S. Alam, T. M. Mosier *et al*., "Modeling a bulb-style Kaplan unit hydrogovernor and turbine in Mathworks-Simulink and RTDS-RSCAD," in *Proceedings of IEEE/PES Transmission and Distribution Conference and Exposition*, New Orleans, USA, Apr. 2022, pp. 1-5.
[36] S. M. S. Alam, A. Banerjee, and T. M. Mosier, "Power hardware-in-the-loop hydropower and ultracapacitor hybrid testbed," in *Proceedings of IEEE PES General Meeting*, Denver, USA. Jul. 2022, pp. 1-5.
[37] W. Du, Z. Chen, K. Schneider *et al*., "A Comparative study of two widely used grid-forming droop controls on microgrid small-signal stability," *IEEE Journal of Emerging and Selected Topics in Power Electronics*, vol. 8, no. 2, pp. 963-975, Jun. 2020.
[38] U. S. Energy Atlas. (2021, Feb.). [Online]. Available: https://atlas. eia. gov/apps/all-energy-infrastructure-and-resources/explore.
[39] S. Shah, H. Sun, D. Nikovski *et al*., "VSC-based active synchronizer for generators," *IEEE Transactions on Energy Conversion*, vol. 33, no. 1, pp. 116-125, Mar. 2018.
[40] D. L. Ransom, "Get in step with synchronization," *IEEE Transactions on Industrial Application*, vol. 50, no. 6, pp. 4210-4215, Nov. -Dec. 2014.

Weihang Yan received the B.S. degree and the M.S. degree in control theory and engineering from School of Information Science and Engineering, Northeastern University, Shenyang, China, in 2014 and 2017, respectively, and the Ph.D. degree in electrical and computer engineering from University of Denver, Denver, USA, in 2020. He is currently a Research Engineer with the Power System Engineering Center, National Renewable Energy Laboratory, Golden, USA. His research interests include renewable energy grid integration, dynamic simulation and stability analysis of power systems with high levels of inverter-based resources.

Vahan Gevorgian received the Ph.D. degree in electrical engineering from the State Engineering University of Armenia, Yerevan, Armenia, in 1993. He joined National Renewable Energy Laboratory (NREL), Golden, USA, in October 1994, and many roles over the years. He is currently working with the Power Systems Engineering Center focused on renewable energy impacts on transmission and interconnection issues and dynamic modeling of variable generation systems. He provides technical support to NREL industry partners and major U.S. wind turbine manufacturers. He is the Member of the IEC Team for wind turbine power quality standards. He was the recipient of multiple Outstanding Individual and Team Staff awards for contributions to NREL Research. His research interests include dynamometer and field testing of large and small wind turbines, dynamometer testing of wind turbine drivetrain components, development of advanced data acquisition systems, and wind turbine power quality.

Przemyslaw Koralewicz is a senior researcher at NREL's Flatiron Campus. He is the project lead for the NREL Controllable Grid Interface (CGI) and oversees multiple power-hardware-in-the-loop experiments involving various megawatt-scale assets including battery, photovoltaic, wind, hydrogen and synchronous generation systems. He helps researchers and industry partners to implement innovative power systems projects featuring newly developed technologies and methods based on the latest research findings. He specializes in development of novel devices characterization methods and utilizing them in hardware validation at NREL's Flatirons Campus. He is also experienced in modeling, stability analysis and validation of smart inverters and complex systems including microgrids.

S M Shafiul Alam received the B. S. and M. S. degrees in electrical and electronic engineering from the Bangladesh University of Engineering and Technology, Dhaka, Bangladesh, in 2008 and 2011, respectively, and the Ph.D. degree in electrical engineering from Kansas State University, Manhattan, USA, in 2015. He is currently a Research Scientist with the Idaho National Laboratory, USA, and works with the Power and Energy Systems Group, EES&T Directorate. His current research interests include reliable and sustainable integration of energy systems, especially the modeling and validation of the operation and control of hybrid energy systems through digital real-time simulation with hardware-in-the-loop testing.

Emanuel Mendiola joined the grid integration team at NREL's Flatirons Campus in 2019. His responsibilities involve controls and protections design for testbed systems, such as NREL's 1 MW/1 MWh battery energy storage systems, used in grid integration research through the SEL real-time automation controller (RTAC) platform and power system modeling with RSCAD. His expertise with the SEL platform includes phasor measurement units, and maintaining an RTAC based site-wide real-time monitoring system for the NREL Flatirons Campus.